Localized slip controlled by dehydration embrittlement of partly serpentinized dunites, Leka Ophiolite Complex, Norway

Kristina G. Dunkel[a,1], Håkon Austrheim[a], François Renard[a,b], Benoit Cordonnier[a], and Bjørn Jamtveit[a]

[a]*Physics of Geological Processes (PGP), Department of Geosciences, University of Oslo, P.O. Box 1048, Blindern, 0136 Oslo, Norway*

[b] *Univ. Grenoble Alpes, ISTerre, F-38000, Grenoble, France*

[1]*kristina.dunkel@geo.uio.no (corresponding author)*

ABSTRACT

Dehydration of partly or completely serpentinized ultramafic rocks can increase the pore fluid pressure and induce brittle failure, a process referred to as dehydration embrittlement. However the extents of strain localization and unstable frictional sliding during deserpentinization are still under debate. In the layered ultramafic sections of the Leka Ophiolite Complex in the Central Norwegian Caledonides, prograde metamorphism of serpentinite veins led to local fluid production and to the growth of Mg-rich and coarse-grained olivine with abundant magnetite inclusions and $\delta^{18}O$ values 1.0-1.5‰ below the host rock. Embrittlement associated with the dehydration caused faulting along highly localized (<10 μm-wide) slip planes near the centers of the original serpentinite veins and pulverization of wall rock olivine. These features along with an earthquake-like size distribution of fault offsets suggest unstable frictional sliding rather than slower creep. Structural heterogeneities in the form of serpentinite veins clearly have first-order controls on strain localization and frictional sliding during dehydration. As most of the oceanic lithosphere is incompletely

serpentinized, heterogeneities represented by a non-uniform distribution of serpentinite are common and may increase the likelihood that dehydration embrittlement triggers earthquakes.

1. INTRODUCTION

Dehydration of serpentine in partly or completely serpentinized ultramafic rocks increases the pore fluid pressure, lowers the effective confining pressure and potentially contributes to brittle failure by dehydration embrittlement and frictional sliding (e.g., Miller et al., 2003; Raleigh and Paterson, 1965). This process can operate at confining pressures where the total volume change during deserpentinization is positive (Dobson et al., 2002), but possibly also at higher pressures (Jung et al., 2004). The breakdown of serpentine has thus been suggested as one possible mechanism for intermediate-depth earthquakes (50–300 km) in subduction zones (e.g., Hacker et al., 2003; Peacock, 2001). However, experimental studies of deserpentinization have produced ambiguous results regarding strain localization and sliding mode. There is evidence for both unstable (Dobson et al., 2002; Jung et al., 2009) and stable sliding (Chernak and Hirth, 2011; Gasc et al., 2011). Unstable sliding involves an acceleration of the slip towards a dynamic velocity, leading to earthquake nucleation and seismic slip. Due to the discrepancies in the experimental results, the role of deserpentinization in triggering seismogenic failure is still under discussion (Proctor and Hirth, 2015, and references therein).

A relevant issue in this discussion is the role of pre-existing heterogeneities (i.e., fractures, veins, remnant clasts of ultramafic rocks) in the lithologies undergoing slip. Most experiments are carried out in almost pure serpentinite with limited heterogeneities beyond the grain scales. In natural systems however, ultramafic rocks are frequently only partly serpentinized and serpentinization is often focused along fractures or other well-defined zones where fluids gained access to the olivine-rich rocks. These features represent heterogeneities on much larger scales than the grain size. Here we describe an example of partly serpentinized

dunites from the Leka Ophiolite Complex (Norway), where dehydration of the serpentinized volumes led to brittle failure and possibly frictional sliding along pre-existing heterogeneities.

2. GEOLOGICAL SETTING

The Leka Ophiolite Complex crops out on the island of Leka in Nord-Trøndelag, Norway (Fig. 1A), and represents part of the Upper or Uppermost Allochthon of the Norwegian tectonostratigraphy. The ophiolite, whose mafic and ultramafic components crystallized at 497 ± 2 Ma (U/Pb zircon age, Dunning and Pedersen, 1988), formed in a supra-subduction zone setting of the North Iapetus ocean (Furnes et al., 1988). It was obducted during the Caledonian orogeny in Ordovician to early Silurian times (Dunning and Pedersen, 1988) and now occurs in a pull-apart structure resulting from post-orogenic extension (Titus et al., 2002). A dehydration event was proposed for the Leka Ophiolite Complex based on olivine pseudomorphs after serpentinized orthopyroxene in the mantle tectonites (Plümper et al., 2012). Correspondingly, radiogenic and stable isotope compositions of talc-carbonate alteration products in the ultramafic cumulates suggest introduction of fluids derived from deserpentinization of underlying units (Bjerga et al., 2015).

The exact timing and cause of the dehydration event is uncertain, but cross-cutting relationships show that it preceded late lizardite- and antigorite-serpentinization. Plümper et al. (2012) proposed that dehydration may have occurred transiently within the oceanic lithosphere before the obduction of the ophiolite. They excluded contact metamorphism, subduction, and Barrovian-type metamorphism during orogeny as causes for deserpentinization based on the absence of magmatic intrusions, the lack of blueschist- and/or eclogite-facies associations, and the transient nature of the dehydration, respectively, and gave several alternatives to explain the temperature increase required for deserpentinization: Faults may have juxtaposed serpentinized mantle against the hotter end of an adjacent ridge segment. The feedback between mantle hydration and hydrothermal convection at oceanic

spreading centers could have led to transient dehydration. Subduction of an active spreading center may have caused the influx of hot asthenosphere through a "slab window" (Shervais, 2001). Here, we present evidence for deserpentinization and associated faulting from a stratigraphically lower part of the ultramafic cumulates than has been investigated by Bjerga et al. (2015) and show that dehydration embrittlement has led to localized slips with earthquake-like properties.

3. METHODS

In the field (WGS84 65.10530, 11.63318; Fig. 1A), fault offsets were measured and hand samples and minicores were taken, from which thin sections were made. From selected samples, major element compositions were measured by wavelength-dispersive spectrometry (WDS) with a Cameca SX 100 electron microprobe (Department of Geosciences, University of Oslo), using an acceleration voltage of 15 kV and beam currents between 10 and 20 nA. Iron distribution maps were acquired using WDS on the Cameca SX 100 electron microprobe and using energy-dispersive spectrometry (EDS) on a Hitachi SU5000 FE-SEM (Department of Geosciences, University of Oslo).

Crystallographic orientation data was obtained from electron backscatter diffraction (EBSD) measurements with the CamScan X500FE Crystal Probe at Géosciences Montpellier (CNRS-Université de Montpellier, France), equipped with an Oxford/Nordlys EBSD detector. The Crystal Probe was operated at an accelerating voltage of 20 kV and a working distance of 25 mm. EBSD patterns were indexed automatically using the AZtec software from Oxford Instruments. Crystallographic preferred orientations (CPOs) and grain boundaries were computed using the Matlab toolbox MTEX (version 4.0.11; http://mtex-toolbox.github.io; Bachmann et al., 2010; Bachmann et al., 2011). Grains were modeled with a misorientation threshold of 10°; grains smaller than 10 pixels were excluded. Non-indexed pixels have been

included in the grains to reconstruct the grain distribution before the fragmentation of olivine grains by late serpentine.

For detailed imaging of a fault zone, one three-dimensional micro-computed X-ray tomographic volume of a 4.0 x 0.9 x 0.7 cm^3 sample was acquired at the beamline ID19 of the European Synchrotron Radiation Facility in Grenoble, with a spatial resolution equal to the voxel size of 4.66 µm. Tomographic acquisition was performed under continuous rotation of the sample with camera synchronization based on the angular encoder signal of the rotation stage. The exposure time was 0.05 s, the beam energy was 68 keV, and 6000 projections were taken over 360°, resulting in a total scan time of about 6 minutes. Tomographic reconstruction was performed using the program PyHST2 (Mirone et al., 2014).

Oxygen isotope analyses were conducted to elucidate the conditions of vein formation. The preparation and analysis of two samples were performed in the NordSIM ion microprobe laboratory at the Swedish Natural History Museum, Stockholm. The samples and standards (San Carlos olivine with $\delta^{18}O = 5.30‰$) were embedded into epoxy resin, polished, and gold-coated. $^{18}O/^{16}O$ isotope ratios were determined *in situ* using secondary ionization mass spectrometry (SIMS) on a CAMECA IMS 1280 ion microprobe, operating with a Cs^+ beam with a spot size of 10 µm, closely following the methodology described for zircon $\delta^{18}O$ by Heinonen et al. (2015). All $\delta^{18}O$ values are given in VSMOW (Vienna Standard Mean Ocean Water).

4. RESULTS

4.1 Structure of the deformed veins

In the layered ultramafites of the Leka Ophiolite Complex, the magmatic layering is displaced along a system of dextral faults by up to 100 m. On an outcrop scale, the displacement recorded by centimeter-thick chromite layers in dunite can reach several tens of centimeters and the faults are clearly localized within well-defined veins (Figs. 1B and 1C).

The veins occur in two sets: one striking approximately N-S and dipping ca. 40° to the east, the other one striking E-W, dipping vertically. Deformation occurs in both sets, with sharp faults in the vein centers (Fig. 2). The veins are irregularly spaced (Fig. 1) with distances of one cm to tens of centimeters.

Four microstructural domains have been defined in these rocks (Fig. 3): Domain A is the host rock, a chromite-bearing dunite composed of several-millimeter-sized olivine porphyroclasts with sharp, parallel subgrain boundaries and neoblasts with an average diameter of 68 µm (grain sizes were calculated from electron-backscatter diffraction maps, Dunkel et al., in prep.). Domain B comprises the veins and consists of coarse-grained olivine (average diameter 127 µm) rich in small magnetite inclusions, which give the veins a dark appearance in the field (Figs. 1B and 1C). The magnetite inclusions are elongated. Examination under cross-polarized light shows that their long axes are oriented parallel to an extinction position of olivine.

Where faults are situated in the veins, strain is strongly localized on discrete slip surfaces in the vein centers. Domain C refers to the fine-grained olivine (average diameter 61 µm) surrounding these slip surfaces. Some of the small grains occur in domains of similar crystallographic orientation (CPO-domains, Dunkel et al., in prep.), indicating that they formed by deformation of a larger precursor grain. Rare larger olivine grains in domain C contain magnetite inclusions such as in domain B. The boundary between domains B and C is sharp; there is no gradual change in grain size. Some faults are filled with coarse-grained (average diameter 128 µm), optically clear olivine constituting domain D. In this case, the chromite layers are displaced not only parallel to the fault, but also perpendicular to it.

A similar crystallographic preferred orientation has been observed for domains A to C (Fig. 3B). A slight rotation (less than 15°) may have occurred between domains B and C, parallel to the macroscopically observed shear sense. The maxima of the orientation

distribution functions are not well enough defined to ensure that the difference in preferred orientation between domains B and C is real, though.

In some cases olivine CPO-domains appear to be slightly stretched across domain C, parallel to the movement recorded by the chromite layers. This reflects minor shear strain in domain C, but the major offset is still accommodated by the central fault. Similarly, chromite grains close to the fault are fragmented, but not sheared (Fig. 4). The strong strain localization on the faults is also illustrated by the sharp displacement of chromite-rich bands imaged by micro-tomography (Fig. 2). The slip plane itself is difficult to image as it is often thinner than the voxel size of the data (4.66 μm), but appears to be about 2-4 μm wide. It is highlighted by 10-100 μm sized fragments of chromite, which are more competent than the surrounding olivine and have been dragged along the fault plane during slip. The slip plane often splits into several branches forming shear duplexes. The slip plane thickness remains similar for every branch.

4.2 Mineral chemistry

The average forsterite (Fo) percentage (Mg/[Mg+Fe]) of olivine (based on 226 point analyses) rises from domain A to domains C and D (Fig. 3), from 92.6 (SD = 0.5, A) over 93.5 (SD = 2.4, B) to 95.1 (SD = 0.9, C) and 95.2 (SD = 1.0, D). The compositions of the olivine in domain B are highly variable and range from Fo87.0 to Fo97.8. The highest Fe contents are probably caused by small magnetite inclusions in the analyzed volume. Many grains in domain B exhibit a diffuse compositional zonation with Fe-rich cores surrounded by Fe-poor rims. The average Fe-content of olivine within domain B decreases towards the vein center (Fig. 3). In general, the olivine compositions in domain C are more homogeneous, but the largest grains in C may show similar grain-internal variations as the olivine in domain B. All microstructural domains are overprinted by late lizardite and antigorite serpentinization as described in Plümper et al. (2012).

The dunites contain Mg, Al-chromite with an average composition of $[Fe^{2+}_{0.61}Mg_{0.38}Mn_{0.01}]Cr_{1.56}Al_{0.32}Fe^{3+}_{0.11}O_4$ (called chromite in the following). Within domain A, chromites are mostly idiomorphic and have thin rims of an Al-poor, Fe-rich spinel phase with an average composition of $[Fe^{2+}_{0.83}Mg_{0.15}Mn_{0.01}Ni_{0.01}]Cr_{0.84}Al_{0.02}Fe^{3+}_{1.13}O_4$ (Cr-magnetite in the following). In domains B and C, the alteration rims are thicker and comprise ferritchromite (with variable compositions between chromite and Cr-magnetite) as well as Cr-magnetite. Along the central fault, chromite is fractured, extensively altered, and sometimes strongly fragmented (Fig. 4). The resulting small particles are mostly Cr-magnetite, with occasional cores of chromite or ferritchromite preserved. Magnetite also occurs as small (max. length 5 µm), prismatic inclusions in olivine in domains B and, subordinately, C. No other phases are associated with these inclusions.

See the supplementary table for all measured mineral compositions.

4.3 Oxygen isotopes

To better constrain the origin of the olivine veins, oxygen isotope profiles with a total of 159 point measurements were acquired across three veins in two samples. Olivine of the host (domain A) has a mean oxygen isotope composition of $\delta^{18}O = 5.10‰$ (SD = 0.30‰), which is in the range of typical mantle peridotite (Mattey et al., 1994). The $\delta^{18}O$ of olivine in domain B is lower, with a mean of 4.16‰ (SD = 0.38‰). The change in $\delta^{18}O$ values from domain A to domain B is sharp (Fig. 5). Values for domains C and D are slightly higher than for B, with 4.25‰ (SD = 0.20‰) and 4.28‰ (SD = 0.20‰), respectively. See the supplementary table for all measured oxygen isotope ratios. A matrix effect (*i.e.*, the dependence of the instrumental mass fractionation on the sample chemistry) of the Fe content of olivine on the oxygen isotope data (e.g., Eiler et al., 1997) can be excluded because there is no correlation between Fe and $\delta^{18}O$ of olivine within the individual domains.

4.4 Fault offsets

The offset of 508 faults within E-W striking veins was recorded by measuring the relative offset of chromite layers cut by the faults (e.g., Fig. 1B). In total, faults were recorded along a (chromite-) layer length of 24.6 m. Without markers, no exact measurements were possible in the N-S striking veins, but the offset seems to be much smaller there. The deformation in these veins may be comparable to tensile bridges (as described by Hoogerduijn Strating and Vissers, 1991) linking the E-W faults. In a bi-logarithmic plot, a linear fit to the size distribution of the measured offsets gives a slope (m) of -1.97 ± 0.27 (Fig. 6, supplementary table). The fitting was performed using a goodness-of-fit method, as described by Clauset et al. (2009), which allows for estimating the slope of a power law, the error on this slope, and the range of fault offsets over which the power law fit is reliable. This method shows that only offsets larger than or equal to 9 mm can be used for the calculation of the slope, as smaller offsets are under-represented, likely because of difficulties recognizing some faults with sub-centimeter displacement or less in the field. Additionally, the relative measurement errors are large for the smallest offsets. The microstructures present no reason to suspect that multiple slip events occurred on one given fault.

5. DISCUSSION

5.1 Formation of olivine veins by deserpentinization

The high and strongly varying forsterite content of olivine in domains B and C and the abundance of magnetite inclusions are characteristic for olivine formed by deserpentinization (e.g., Arai, 1975). The main reason for the compositional heterogeneities is the metasomatic growth of Fe-poor prograde olivine on Fe-richer primary olivine (Arai, 1975; Nozaka, 2003). The increase in variability and average Fe-content from the inner to the outer part of domain B (Fig. 3) can be explained by a decreasing degree of serpentinization towards the host rock.

As olivine has straight extinction, the orientation of the magnetite inclusions parallel to an extinction position of olivine shows that they are aligned with crystallographic directions of olivine. This could conceivably indicate exsolution of magnetite from the fayalite component of the olivine due to decompression, cooling or oxidation processes (see Franz and Wirth (2000) for an overview over models explaining the formation of spinel inclusions in olivine) instead of incorporation in growing prograde olivine. However, as there are neither other inclusions (which could balance the silicate content during magnetite exsolution from olivine) nor evidence of a high-pressure event (during which Fe^{3+}-bearing olivine could have been stable), the direct formation of magnetite from the fayalite component of olivine can be excluded. Instead, we assume that the magnetite crystals were aligned during incorporation into the growing olivine to minimize the surface energy.

The change in oxygen isotope ratios from the host to the vein (Figs. 5 and 7) supports the influence of a fluid phase. The veins acted as preferential pathways for fluid infiltration during serpentinization and fluid escape during deserpentinization. Because the dehydration of serpentine leads to an ^{18}O-enrichment of the rock (Ivanova et al., 2013; Mayeda and Clayton, 1998), the vein serpentine had a $\delta^{18}O$ value lower than 4.2‰, the approximate oxygen isotope ratio of the prograde olivine (domains B and C). This is below the initial $\delta^{18}O$ of the rock (5.1‰, domain A), implying that the dunites were depleted in ^{18}O during serpentinization. Assuming a seawater composition of the reacting fluid, serpentinization at temperatures above 200°C causes an ^{18}O-depletion (Alt et al., 2007). Using the empirical serpentine-water fractionation factor from Saccocia et al. (2009), $\delta^{18}O < 4.2$‰ indicates a serpentinization temperature $T > 230$ °C. The variations in $\delta^{18}O$ in domain B reflect the presence of relics of primary olivine, similar to the variations in the forsterite content.

The exact composition of the former serpentinite veins is unknown, but it is likely that they comprised brucite in addition to serpentine and magnetite, and that antigorite and brucite

were subsequently dehydrated to olivine. Without the presence of brucite, talc (or, at higher confining pressure, pyroxene) should form in addition to olivine during the dehydration reaction. As no phases apart from olivine, chromite and its alteration products, magnetite, and late serpentine have been observed in the veins, brucite was probably present in the serpentinite veins before the prograde metamorphism.

Thin Cr-magnetite rims around chromite are common in serpentinized ultramafites (Barnes, 2000), and their occurrence in all domains can be related to the late serpentinization. The intermediate compositions of chromite alteration products (ferritchromite) in domains B and C (Fig. 4), however, indicate temperatures above the miscibility gap between chromite and magnetite at 500-600 °C (Barnes, 2000). This supports that the temperatures were sufficiently high for deserpentinization, which occurs at ca. 450-600 °C for pure antigorite, and at ca. 350-450 °C for antigorite and brucite, depending on the pressure (Evans, 2004). The chromite in domain A experienced the same temperatures, but did not react because of the absence of fluids.

Olivine veins that formed by the dehydration of serpentinite veins are a previously unreported type of prograde olivine occurrence. The initially low degree of serpentinization distinguishes them from olivine veins in serpentinite units (e.g., Healy et al., 2009) and from large prograde peridotite bodies with sharp contacts towards the relict serpentinite (e.g., Khedr and Arai, 2012; Padrón-Navarta et al., 2011).

5.2 Deformation accompanying deserpentinization

The similarity between the few large olivine grains in domain C and the olivine in domain B, including abundant magnetite inclusions and varying forsterite content, suggests that C formed by fragmentation of B. The sharp contacts between domains B and C (Fig. 3) and the high degree of localization of the fault itself, as documented by the sharp offset of chromite visible in microtomographic images (Fig. 2), indicate that the fragmentation was

brittle. Another possibility would be that the olivine in domain C recrystallized and that the fine grain size is due to Zener pinning by magnetite. However, it is unlikely that recrystallization occurred exclusively in domain C. Recrystallization can be enabled by a fluid phase, which was clearly present in both domains and not only in domain C, and/or by an increase in temperature. Frictional heating could possibly have affected only domain C, but back-of-the-envelope calculations show that the temperature difference between host rock and fault zone declines to less than 10 °C within minutes, which is insufficient for recrystallization of olivine.

A random distribution of low-angle misorientation rotation axes in domain C (Dunkel et al., in prep.) also contradicts subgrain rotation recrystallization and bulging recrystallization, both of which could have caused the small grain size in domain C. Grain boundary sliding results in random misorientation rotation axes, but could not explain the grain size reduction from domain B to C. We therefore assume that brittle deformation caused the grain size reduction.

Faulting could potentially have happened independently of the dehydration. However, if dehydration was complete before the faulting, there would have been no reason for the faults to localize in the vein centers. Localization would have occurred either in the finer-grained, weaker host rock, or at the rheological boundaries between fine-grained host and coarse-grained vein (as described by Mancktelow and Pennacchioni (2005) for the localization of ductile shear zones), and not within the more competent veins. Additionally, as both the host rock and the veins are uniformly affected by later lizardite and antigorite serpentinization, the faulting occurred prior to obduction of the ophiolite.

The concurrency of brittle faulting and deserpentinization indicates dehydration embrittlement as the reason for the failure. Domain D, consisting of inclusion-free, coarse-grained olivine, did not form by recrystallization or deformation of olivine corresponding to

domains A to C, but directly from a fluid in a dilational setting, as shown by the fault-perpendicular displacement of the chromite layers. This demonstrates the locally high fluid pressure along the fault.

5.3 Timing and mechanism of dehydration embrittlement

In the Leka Ophiolite Complex, faulting occurred when dehydration was at an advanced stage. Otherwise, domain C could not have formed by deformation of domain B. This is a major difference to many experimental results, which indicate that slip occurs at the early stages of deserpentinization (e.g., Dobson et al., 2002; Jung et al., 2004; Jung et al., 2009). This may be related to the initial amounts and distributions of serpentine and olivine: As pointed out by Leclère et al. (2016), in a dehydration reaction in which only the product phase shows velocity-weakening behavior, the stability of slip is related to the spatial distribution of the product. This is the case for olivine at temperatures below 600 °C (Boettcher et al., 2007), implying that, for the Leka Ophiolite, the presence of olivine in the host rock and in the core of the slip zone favored velocity-weakening behavior, and therefore seismic sliding. The different distributions and relative amounts of serpentine and olivine in a dehydrating, locally serpentinized peridotite, compared to a dehydrating fully serpentinized rock, are probably the reasons for the strain localization in this case. When a partly serpentinized dunite is progressively dehydrated, most of the host rock remains strong and does not fail immediately. Only at an advanced stage of dehydration will the fluid pressure be high enough to trigger failure.

An alternative is that faulting, rather than being triggered by a decrease in effective normal stress during an early increase in pore fluid pressure, was related to a late fluid overpressure pulse following a collapse of reaction-induced porosity. When deserpentinization is advanced, the permeability of the rock is much higher than in the beginning (Tenthorey and Cox, 2003) due to the decrease in solid volume. The pore fluid

pressure, which was presumably high during initial deserpentinization, may consequently have declined during progressive dehydration. A collapse of the porosity after fluid drainage may finally have caused a pulse in fluid overpressure, as described for gypsum dehydration by Leclère et al. (2016). This in turn could have led to faulting and deformation of the prograde olivine. Based on the observed microstructures, none of the two possibilities can be ruled out.

5.4 Stable versus unstable sliding

Although numerous studies have proposed that deserpentinization may trigger seismic slip and earthquakes (Dobson et al., 2002; Jung et al., 2009), recent deformation experiments indicate that dehydration of homogeneous antigorite serpentinite subjected to differential stress does not produce unstable frictional sliding, but a semi-brittle, distributed mode of deformation (Proctor and Hirth, 2015). During deserpentinization in the Leka Ophiolite Complex, faulting was clearly not distributed, occurred along well-defined slip surfaces, and may have been unstable. Although there is, in the absence of frozen frictional melts, no unequivocal evidence for seismic slip in these rocks, circumstantial evidence, namely strain localization, 'pulverization' of olivine, and an earthquake-like size distribution of fault offsets, suggests unstable sliding. These three pieces of evidence are discussed below.

An essentially constant crystallographic preferred orientation of olivine, equal to that of the host rock, is a characteristic feature of all domains in the deformed veins described above (Fig. 3B). The preservation of the mantle fabric (of domain A) in the veins (domain B) can be attributed to epitaxial growth of prograde olivine on relics of primary olivine (Dunkel et al., in prep.). Extensive shear movement would have weakened the fabric from domain B to C, but this is not the case. Neither are the chromite layers bent towards the central fault plane (Fig. 2). Most of the strain was accommodated by slip on discrete fault planes while the surrounding areas (domain C) experienced grain-size reduction without significant internal shearing. While strong strain localization alone does not necessarily reflect unstable sliding, a

reduction of the grain size by about half the diameter without movement of the grains relative to each other is unlikely to occur during stable sliding. This fragmentation of the prograde olivine without shear is reminiscent of 'rock pulverization', a process which has mostly been used to describe fault damage in the continental upper crust (e.g., Dor et al., 2006; Mitchell et al., 2011), where the pulverization of the rocks by the propagation of a dynamic rupture became obvious by the observation of rock powder in the field. Following the definition of Dor et al. (2006), a 'pulverized rock' is a damaged rock in which the original textures are preserved, in which very little or no shear is visible, and which yields a powdery rock-flour texture when pressed by hand. The first two conditions are met in the deformation zones described above, but the deformed zones are cohesive and cannot be pressed by hand. However, if faulting occurred during serpentine dehydration, in the olivine stability field, it is likely that some healing occurred after the deformation and olivine fragments were sintered together. Therefore, despite obvious differences between the Leka Ophiolite Complex case and the classical understanding of rock pulverization, a comparable 'pulverization' at higher temperature and confining pressure seems likely. Pulverization is diagnostic for fast rupture velocity and seismic strain rates (Reches and Dewers, 2005; Rowe and Griffith, 2015). Because of the centimeter to decimeter displacement, one can assume sub-Rayleigh velocity for a dynamic rupture in these rocks, which has propagated and generated damage and modification of the elastic properties at the rupture tip, changing the rock into a granular material (Xu et al., 2015). This would then be the origin of the pulverized domain C observed in both tomography and EBSD data (Figs. 2 and 3).

The third argument for seismic slip is the earthquake-like size distribution of the faulting events in the Leka Ophiolite Complex (Fig. 6). The global size distribution of earthquakes on Earth shows a power law behavior commonly described by the Gutenberg-

Richter relationship, which states that the number of earthquakes N with a magnitude larger than or equal to M is proportional to M according to:

$log(N) \sim -bM$, (1)

where b is a constant, commonly referred to as the *b*-value. For incremental rather than cumulative earthquake distributions, this relationship becomes (Clauset et al., 2009):

$log(n) \sim -(b+1)M$, (2)

with n being the number of earthquakes of magnitude M. Based on empirical data, Wells and Coppersmith (1994) found that the moment magnitude *M* is proportional to the average displacement *d* on a fault:

$M \sim 0.82 * log(d)$, (3)

Combining equations (2) and (3) gives

$log(n) \sim -(b+1) * 0.82 * log(d)$. (4)

The slope of a linear regression in a log-log plot of the number of displacements versus displacement is indicative of a power-law relationship with an exponent *m* such that

$m = -0.82 * (b+1)$. (5)

A power law fit to the fault offsets distribution measured in the Leka Ophiolite Complex gives $m = -1.97 \pm 0.27$, so that $b = 1.4 \pm 0.3$ (Fig. 6). The relationship between average fault displacement and magnitude (Eq. 3) is not well constrained, meaning that the calculated *b*-value should only be taken as an approximate value. Nevertheless, it falls within the range of 0.6 to 1.3 for *b*-values in regional earthquake catalogs (Udías, 1999). Moreover, *b*-values higher than the global average of $b = 1$ on Earth are also typically observed in heterogeneous rocks or where fluid injection and extractions are performed (see 5.5).

5.5 Effects of heterogeneities

As stated above (5.3), the mechanical response of a locally serpentinized, strong dunite to dehydration will be different than that of a weaker fully serpentinized rock.

Therefore, it is not surprising that although strain may be distributed during dehydration of homogeneous serpentinite, it becomes strongly localized in a heterogeneous rock volume where fluid pressure is locally increased along pre-existing veins, as it is the case in the Leka Ophiolite Complex. Heterogeneities play a major role during material failure (e.g.,Vasseur et al., 2015) because they reduce the overall material strength and thus the maximum differential stress to rupture, and shift the relative size distribution of seismic events, represented by the *b*-value, to a larger proportion of small earthquakes (Scholz, 1968). Such a change in size distribution of earthquakes towards higher *b*-values has been produced by local injection-induced fluid pressure increases during enhanced geothermal system experiments (Bachmann et al., 2012). We propose here that it is likewise expected for earthquakes triggered by dehydration embrittlement in heterogeneously serpentinized peridotites. Mapping of *b*-values along convergent plate margins has indeed demonstrated a correlation between regions undergoing fluid production by dehydration reactions and high *b*-values in the range of 1.3 to 1.6 (Singh and Singh, 2015; Wiemer and Benoit, 1996). The deformation in the Leka Ophiolite Complex probably did not occur in a convergent margin setting and the confining pressure was lower; nevertheless the empirical *b*-value of 1.4 determined for the faulting in the Leka Ophiolite Complex is in accordance with these observations

Recent deformation experiments on partially hydrated peridotite samples also suggest that the mode of faulting is dependent on the ratio of serpentinite to olivine, and earthquakes are most likely to occur in partly hydrated peridotites, which are capable of sustaining larger bulk strengths than pure serpentinites (Ferrand et al., in review). As the mantle lithosphere is only partly serpentinized (17-31%, Garth and Rietbrock, 2014) and the distribution of serpentine is almost invariably heterogeneous and focused on faults and fractures where aqueous fluids have gained access to the ultramafic rocks, the discussion of the feasibility of

dehydration embrittlement and earthquakes triggered by deserpentinization should focus on heterogeneous rather than homogeneous systems.

6. CONCLUSIONS

Microstructural and mineralogical evidence demonstrate that olivine veins in dunites from the Leka Ophiolite Complex formed by dehydration of serpentinite veins. Faults with sharp slip surfaces are localized in these veins and are surrounded by millimeter-thick zones of fine-grained olivine, which formed by brittle deformation of the surrounding coarser-grained olivine vein.

We envisage the following history of these veins (Fig. 7): Fluids infiltrated a chromite-bearing dunite along fractures and led to a hydration of olivine around the fractures. During later prograde metamorphism, serpentine was dehydrated and new olivine grew. Dehydration embrittlement, as a consequence of a reduction in effective normal stress due to a local increase in fluid pressure during deserpentinization, resulted in localized slip in the vein centers, displacing chromite layers, and to a pulverization of the prograde olivine adjacent to the fault plane.

This study stresses the importance of heterogeneities (here: serpentinite veins in dunite) in controlling localized frictional sliding, and possibly the size distribution of seismic events, during deformation of partly serpentinized mantle rocks.

ACKNOLWEDGEMENTS

This project has been supported by the People Programme (Marie Curie Actions) of the European Union's Seventh Framework Programme FP7/2007-2013/ under REA-Grant Agreement No. 608001, 'ABYSS', and by the European Union's Horizon 2020 Research and Innovation Programme under the ERC Advanced Grant Agreement No. 669972, 'Disequilibirum Metamorphism' ('DIME'), to BJ. The NordSIM facility is jointly funded by Denmark, Sweden and Iceland (this is Nordsim publication # 490). We thank Benoit

Ildefonse, Muriel Erambert, and Martin Whitehouse for help with the EBSD, EMP, and oxygen isotope analysis, respectively. We appreciate the valuable comments of two anonymous reviewers.

REFERENCES

Alt, J.C., Shanks, W.C., Bach, W., Paulick, H., Garrido, C.J., Beaudoin, G., 2007. Hydrothermal alteration and microbial sulfate reduction in peridotite and gabbro exposed by detachment faulting at the Mid-Atlantic Ridge, 15°20′N (ODP Leg 209): A sulfur and oxygen isotope study. Geochemistry, Geophysics, Geosystems 8, Q08002, doi:10.1029/2007GC001617.

Arai, S., 1975. Contact metamorphosed dunite-harzburgite complex in the Chugoku district, western Japan. Contributions to Mineralogy and Petrology 52, 1-16, doi: 10.1007/BF00377998.

Bachmann, C.E., Wiemer, S., Goertz-Allmann, B., Woessner, J., 2012. Influence of pore-pressure on the event-size distribution of induced earthquakes. Geophysical Research Letters 39, L09302, doi:10.1029/2012GL051480.

Bachmann, F., Hielscher, R., Schaeben, H., 2010. Texture analysis with MTEX–free and open source software toolbox. Solid State Phenomena 160, 63-68, doi: 10.4028/www.scientific.net/SSP.160.63.

Bachmann, F., Hielscher, R., Schaeben, H., 2011. Grain detection from 2d and 3d EBSD data—Specification of the MTEX algorithm. Ultramicroscopy 111, 1720-1733, doi:10.1016/j.ultramic.2011.08.002.

Barnes, S.J., 2000. Chromite in komatiites, II. Modification during greenschist to mid-amphibolite facies metamorphism. Journal of Petrology 41, 387-409, doi: 10.1093/petrology/41.3.387.

Bjerga, A., Konopásek, J., Pedersen, R.B., 2015. Talc–carbonate alteration of ultramafic rocks within the Leka Ophiolite Complex, Central Norway. Lithos 227, 21-36, doi: 10.1016/j.lithos.2015.03.016.

Boettcher, M. S., Hirth, G., and Evans, B., 2007. Olivine friction at the base of oceanic seismogenic zones. Journal of Geophysical Research: Solid Earth 112, B01205, doi: 10.1029/2006JB004301.

Chernak, L.J., Hirth, G., 2011. Syndeformational antigorite dehydration produces stable fault slip. Geology 39, 847-850, doi: 10.1130/G31919.1.

Clauset, A., Shalizi, C. R., Newman, M. E., 2009. Power-law distributions in empirical data. SIAM Review 51, 661-703, doi: 10.1137/070710111.

Dobson, D.P., Meredith, P.G., Boon, S.A., 2002. Simulation of subduction zone seismicity by dehydration of serpentine. Science 298, 1407-1410, doi: 10.1126/science.1075390.

Dor, O., Ben-Zion, Y., Rockwell, T.K., Brune, J., 2006. Pulverized rocks in the Mojave section of the San Andreas Fault Zone. Earth and Planetary Science Letters 245, 642-654, doi: 10.1016/j.epsl.2006.03.034.

Dunning, G.R., Pedersen, R.B., 1988. U/Pb ages of ophiolites and arc-related plutons of the Norwegian Caledonides: implications for the development of Iapetus. Contributions to Mineralogy and Petrology 98, 13-23, doi: 10.1007/BF00371904.

Eiler, J.M., Graham, C., Valley, J.W., 1997. SIMS analysis of oxygen isotopes: matrix effects in complex minerals and glasses. Chemical Geology 138, 221-244, doi: 10.1016/S0009-2541(97)00015-6.

Evans, B.W., 2004. The serpentinite multisystem revisited: chrysotile is metastable. International Geology Review 46, 479-506, doi: 10.2747/0020-6814.46.6.479.

Franz, L., Wirth, R., 2000. Spinel inclusions in olivine of peridotite xenoliths from TUBAF seamount (Bismarck Archipelago/Papua New Guinea): evidence for the thermal and

tectonic evolution of the oceanic lithosphere. Contributions to Mineralogy and Petrology 140, 283-295, doi: 10.1007/s004100000188.

Furnes, H., Pedersen, R.B., Stillman, C.J., 1988. The Leka Opholite Complex, central Norwegian Caledonides: field characteristics and geotectonic significance. Journal of the Geological Society 145, 401-412, doi: 10.1144/gsjgs.145.3.0401.

Garth, T., Rietbrock, A., 2014. Order of magnitude increase in subducted H2O due to hydrated normal faults within the Wadati-Benioff zone. Geology 42, 207-210, doi: 10.1130/G34730.1.

Gasc, J., Schubnel, A., Brunet, F., Guillon, S., Mueller, H.-J., Lathe, C., 2011. Simultaneous acoustic emissions monitoring and synchrotron X-ray diffraction at high pressure and temperature: Calibration and application to serpentinite dehydration. Physics of the Earth and Planetary Interiors 189, 121-133, doi: 10.1016/j.pepi.2011.08.003.

Hacker, B.R., Peacock, S.M., Abers, G.A., Holloway, S.D., 2003. Subduction factory 2. Are intermediate-depth earthquakes in subducting slabs linked to metamorphic dehydration reactions? Journal of Geophysical Research: Solid Earth 108, 2030, doi: 10.1029/2001JB001129.

Heinonen, A., Andersen, T., Rämö, O.T., Whitehouse, M., 2015. The source of Proterozoic anorthosite and rapakivi granite magmatism: evidence from combined in situ Hf–O isotopes of zircon in the Ahvenisto complex, southeastern Finland. Journal of the Geological Society 172, 103-112. doi:10.1144/jgs2014-013.

Healy, D., Reddy, S.M., Timms, N.E., Gray, E.M., Brovarone, A.V., 2009. Trench-parallel fast axes of seismic anisotropy due to fluid-filled cracks in subducting slabs. Earth and Planetary Science Letters 283, 75-86, doi: 10.1016/j.epsl.2009.03.037.

Hoogerduijn Strating, E.H., Vissers, R.L.M., 1991. Dehydration-induced fracturing of eclogite-facies peridotites: Implications for the mechanical behaviour of subducting oceanic lithosphere. Tectonophysics 200, 187-198, doi: 10.1016/0040-1951(91)90014-J.

Ivanova, M.A., Lorenz, C.A., Franchi, I.A., Bychkov, A.Y., Post, J.E., 2013. Experimental simulation of oxygen isotopic exchange in olivine and implication for the formation of metamorphosed carbonaceous chondrites. Meteoritics & Planetary Science 48, 2059-2070, doi: 10.1111/maps.12204.

Jung, H., Fei, Y., Silver, P.G., Green, H.W., 2009. Frictional sliding in serpentine at very high pressure. Earth and Planetary Science Letters 277, 273-279, doi: 10.1016/j.epsl.2008.10.019.

Jung, H., Green, H.W., Dobrzhinetskaya, L.F., 2004. Intermediate-depth earthquake faulting by dehydration embrittlement with negative volume change. Nature 428, 545-549, doi: 10.1038/nature02412.

Khedr, M.Z., Arai, S., 2012. Petrology and geochemistry of prograde deserpentinized peridotites from Happo-O'ne, Japan: Evidence of element mobility during deserpentinization. Journal of Asian Earth Sciences 43, 150-163, doi: 10.1016/j.jseaes.2011.08.017.

Leclère, H., Faulkner, D., Wheeler, J., Mariani, E., 2016. Permeability control on transient slip weakening during gypsum dehydration: Implications for earthquakes in subduction zones. Earth and Planetary Science Letters 442, 1-12, doi:10.1016/j.epsl.2016.02.015.

Mancktelow, N. S., Pennacchioni, G., 2005. The control of precursor brittle fracture and fluid-rock interaction on the development of single and paired ductile shear zones. Journal of Structural Geology 27, 645-661, doi: 10.1016/j.jsg.2004.12.001.

Mattey, D., Lowry, D., Macpherson, C., 1994. Oxygen isotope composition of mantle peridotite. Earth and Planetary Science Letters 128, 231-241, doi: 10.1016/0012-821X(94)90147-3.

Mayeda, T., Clayton, R., 1998. Oxygen isotope effects in serpentine dehydration, 29th Lunar and Planetary Science Conference, Abstract no. 1405.

Miller, S., Van Der Zee, W., Olgaard, D., Connolly, J., 2003. A fluid-pressure feedback model of dehydration reactions: experiments, modelling, and application to subduction zones. Tectonophysics 370, 241-251, doi:10.1016/S0040-1951(03)00189-6.

Mirone, A., Brun, E., Gouillart, E., Tafforeau, P., Kieffer, J., 2014. The PyHST2 hybrid distributed code for high speed tomographic reconstruction with iterative reconstruction and a priori knowledge capabilities. Nuclear Instruments and Methods in Physics Research Section B: Beam Interactions with Materials and Atoms 324, 41-48, doi:10.1016/j.nimb.2013.09.030.

Mitchell, T.M., Ben-Zion, Y., Shimamoto, T., 2011. Pulverized fault rocks and damage asymmetry along the Arima-Takatsuki Tectonic Line, Japan. Earth and Planetary Science Letters 308, 284-297, doi: 10.1016/j.epsl.2011.04.023.

Nozaka, T., 2003. Compositional heterogeneity of olivine in thermally metamorphosed serpentinite from Southwest Japan. American Mineralogist 88, 1377-1384, doi: 10.2138/am-2003-8-922.

Padrón-Navarta, J.A., Sánchez-Vizcaíno, V.L., Garrido, C.J., Gómez-Pugnaire, M.T., 2011. Metamorphic record of high-pressure dehydration of antigorite serpentinite to chlorite harzburgite in a subduction setting (Cerro del Almirez, Nevado–Filábride Complex, Southern Spain). Journal of Petrology 52, 2047-2078, doi: 10.1093/petrology/egr039.

Peacock, S.M., 2001. Are the lower planes of double seismic zones caused by serpentine dehydration in subducting oceanic mantle? Geology 29, 299-302, doi: 10.1130/0091-7613(2001)029<0299:ATLPOD>2.0.CO;2.

Pedersen, R.-B., Johannesen, G.M., Boyd, R., 1993. Stratiform platinum-group element mineralizations in the ultramafic cumulates of the Leka Ophiolite Complex, central Norway. Economic Geology 88, 782-803, doi: 10.2113/gsecongeo.88.4.782.

Plümper, O., Piazolo, S., Austrheim, H., 2012. Olivine pseudomorphs after serpentinized orthopyroxene record transient oceanic lithospheric mantle dehydration (Leka Ophiolite Complex, Norway). Journal of Petrology 53, 1943-1968, doi: 10.1093/petrology/egs039.

Proctor, B., Hirth, G., 2015. Role of pore fluid pressure on transient strength changes and fabric development during serpentine dehydration at mantle conditions: Implications for subduction-zone seismicity. Earth and Planetary Science Letters 421, 1-12, doi: 10.1016/j.epsl.2015.03.040.

Raleigh, C., Paterson, M., 1965. Experimental deformation of serpentinite and its tectonic implications. Journal of Geophysical Research 70, 3965-3985, doi: 10.1029/JZ070i016p03965.

Reches, Z., Dewers, T.A., 2005. Gouge formation by dynamic pulverization during earthquake rupture. Earth and Planetary Science Letters 235, 361-374, doi: 10.1016/j.epsl.2005.04.009.

Rowe, C. D., and Griffith, W. A., 2015. Do faults preserve a record of seismic slip: A second opinion. Journal of Structural Geology 78, 1-26, doi: 10.1016/j.jsg.2015.06.006.

Saccocia, P.J., Seewald, J.S., Shanks Iii, W.C., 2009. Oxygen and hydrogen isotope fractionation in serpentine–water and talc–water systems from 250 to 450 °C, 50 MPa. Geochimica et Cosmochimica Acta 73, 6789-6804, doi: 10.1016/j.gca.2009.07.036.

Scholz, C.H., 1968. The frequency-magnitude relation of microfracturing in rock and its relation to earthquakes. Bulletin of the Seismological Society of America 58, 399-415.

Shervais, J. W., 2001. Birth, death, and resurrection: The life cycle of suprasubduction zone ophiolites. Geochemistry, Geophysics, Geosystems 2, Paper number 2000GC000080, doi: 10.1029/2000GC000080.

Singh, C., Singh, S., 2015. Imaging b-Value Variation beneath the Pamir–Hindu Kush Region. Bulletin of the Seismological Society of America 105, 808-815, doi: 10.1785/0120140112.

Tenthorey, E., Cox, S.F., 2003. Reaction-enhanced permeability during serpentinite dehydration. Geology 31, 921-924, doi:10.1130/G19724.1.

Titus, S. J., Fossen, H., Pedersen, R. B., Vigneresse, J. L., and Tikoff, B., 2002. Pull-apart formation and strike-slip partitioning in an obliquely divergent setting, Leka Ophiolite, Norway. Tectonophysics 354, 101-119, doi: 10.1016/S0040-1951(02)00293-7.

Udías, A., 1999. Principles of seismology, Cambridge, Cambridge University Press, p. 386.

Vasseur, J., Wadsworth, F.B., Lavallée, Y., Bell, A.F., Main, I.G., Dingwell, D.B., 2015. Heterogeneity: The key to failure forecasting. Scientific reports 5, 13259, doi: 10.1038/srep13259.

Wells, D.L., Coppersmith, K.J., 1994. New empirical relationships among magnitude, rupture length, rupture width, rupture area, and surface displacement. Bulletin of the Seismological Society of America 84, 974-1002.

Wiemer, S., Benoit, J.P., 1996. Mapping the b-value anomaly at 100 km depth in the Alaska and New Zealand subduction zones. Geophysical Research Letters 23, 1557-1560.

Xu, S., Ben-Zion, Y., Ampuero, J. P., Lyakhovsky, V. 2015. Dynamic ruptures on a frictional interface with off-fault brittle damage: feedback mechanisms and effects on slip and near-

fault motion. Pure and Applied Geophysics 172, 1243-1267, doi: 10.1007/s00024-014-0923-7.

FIGURES

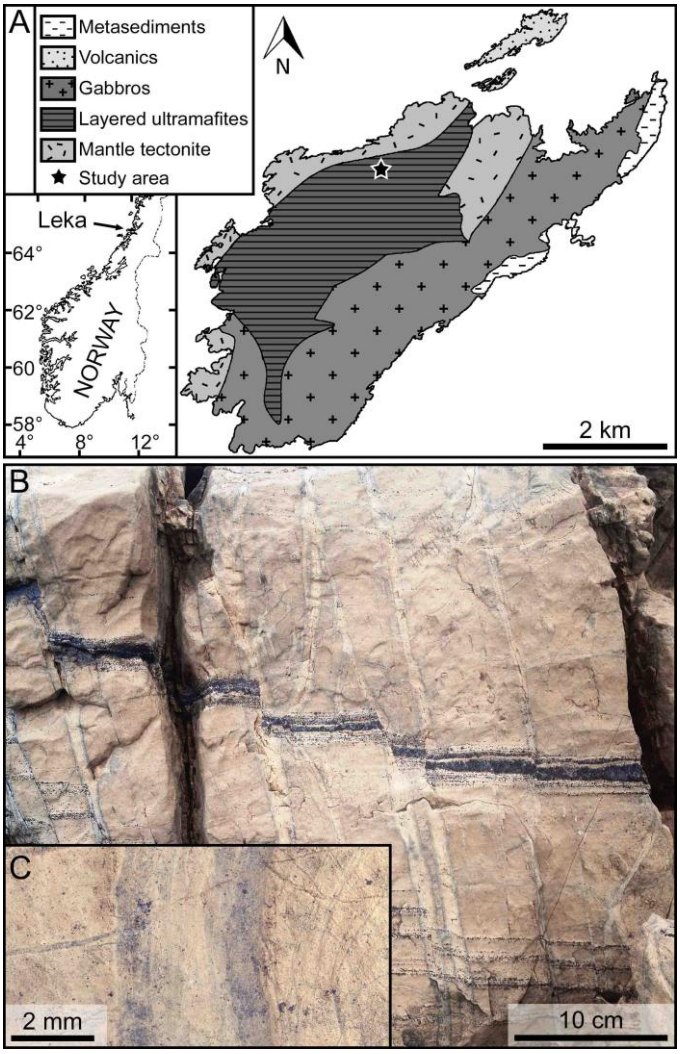

Figure 1. A. Geological map of the Leka Ophiolite Complex (after Pedersen et al., 1993), showing the study area (WGS84 65.10530, 11.63318) in the layered ultramafites. B. Field image of a dunite in which chromite layers (horizontal) record a sharp offset along the centers of olivine veins (vertical). C. Detailed view of one vein, comparable to the area shown in figure 3. The dark edges of the veins are caused by a high density of magnetite inclusions in olivine.

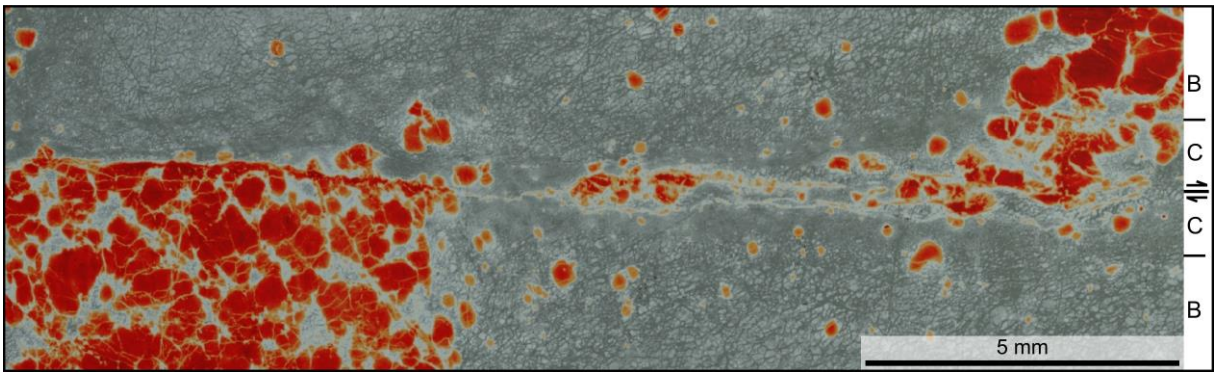

Figure 2. Sharp right-lateral offset of a chromite layer, shown in an X-ray microtomography image. Chromite grains are in red, olivine in light grey, and serpentine in dark grey. The letters on the right side roughly indicate the position of the central slip plane and of domains B and C (see 4.1). Fragmentation of the chromite grains is localized within a 2-4 µm thick slip zone, while the grain size reduction of olivine is observed throughout domain C. (Sample LE11-13)

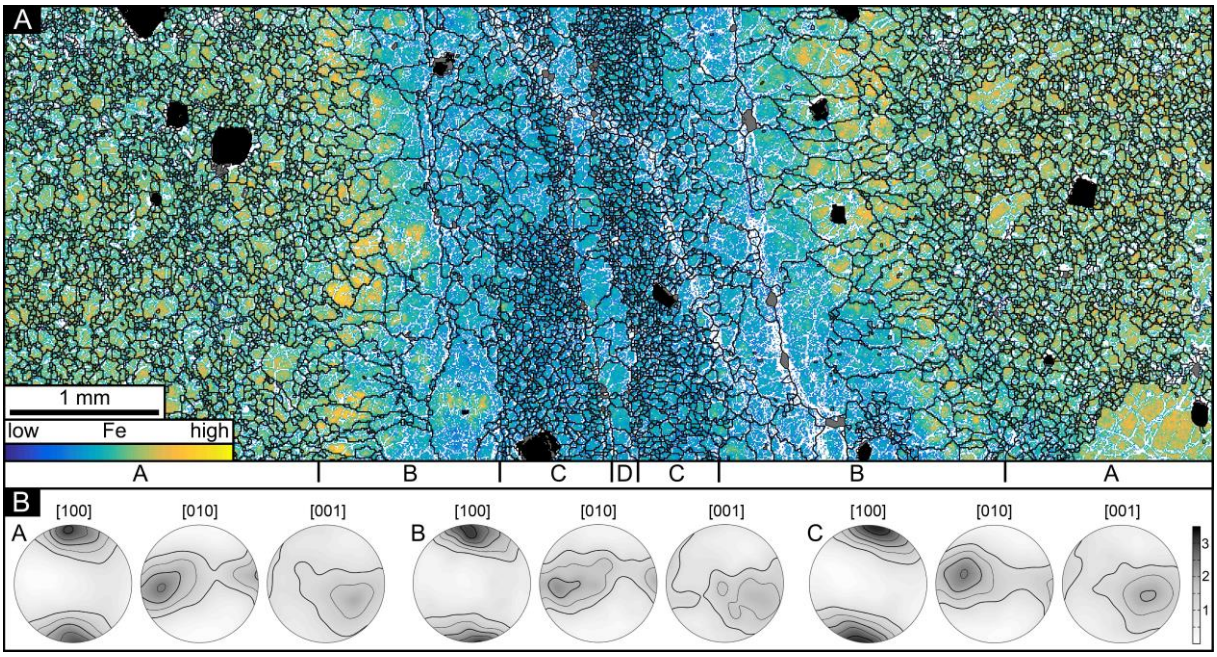

Figure 3. A. Vein structure (grain boundaries computed from EBSD data) and Fe distribution in olivine (EDS element distribution map). Black: chromite, grey: magnetite. White areas are late serpentine veins that have been excluded during grain modeling. Letters on the bottom indicate the positions of domains A to D (see 4.1 for explanations). The fault is located in the center of the vein and filled with olivine of domain D. The shear sense is unknown for this

fault (out of plane). Note the grain size reduction in domain C, interpreted as pulverization due to slip on the fault. B. Pole figures (equal-are projections) of olivine [100], [010], and [001] axes, showing the constant crystallographic orientation in domains A to C. As no foliation or lineation is visible, the thinsection reference frame was used for the pole figures, i.e. the orientation of the stereonets in subfigure B is the same as the orientation of the image in subfigure A. Note that the parallelism of vein orientation and olivine a-axis orientation is a coincidence and not characteristic for all veins. The orientation distribution functions were computed based on the mean orientations of 16130 grains from domain A, 3133 from domain B, and 8705 from domain C. Contours are drawn for multiples of 0.5 of a uniform distribution. (Sample LE05-14)

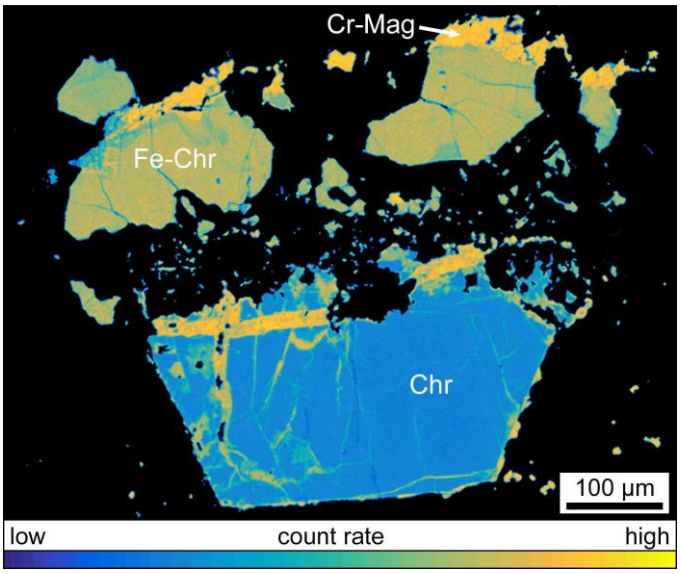

Figure 4. Fragmentation and chemical alteration of an individual chromite grain adjacent to the fault plane, in domain C. WDS element distribution map of Fe in oxide minerals showing increasing alteration (Fe-enrichment) with decreasing distance to the fault plane (located ca. 100 µm above, and parallel to, the upper margin of this figure). Chr: chromite, Fe-Chr: ferritchromite, Cr-Mag: Cr-magnetite. (Sample LE04-14)

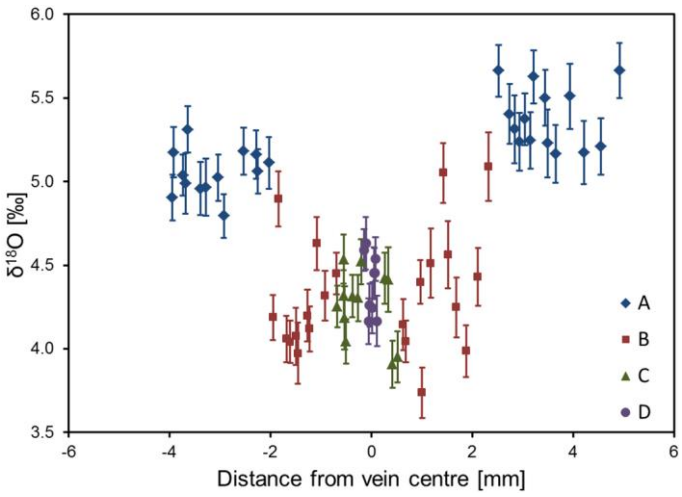

Figure 5. Profile of $\delta^{18}O$ in olivine perpendicular to a vein. Note the sharp change in $\delta^{18}O$ values from the host (A) to the vein (B-D). (Sample LE05-14)

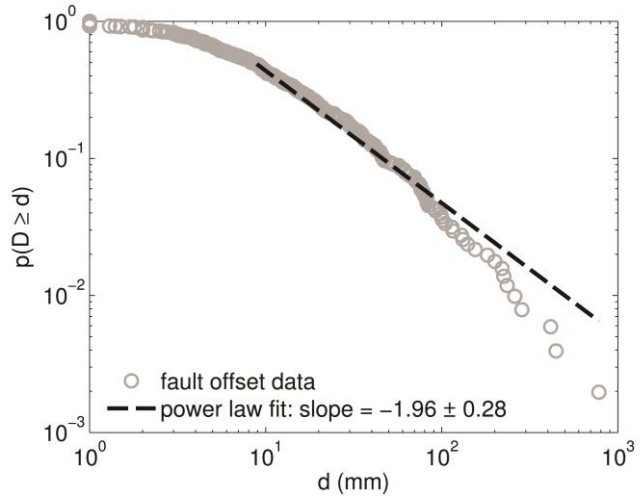

Figure 6. Cumulative frequency distribution of the offsets (d) on 508 E-W striking faults displacing chromite layers in the Leka Ophiolite Complex. Typical chromite layers and fault offsets are shown in Fig. 1B. The calculation of the power law fit was performed using the method described in Clauset et al. (2009) and indicates a slope of -0.97 on the cumulative distribution, corresponding to a slope of $m = -1.97$ on the incremental distribution.

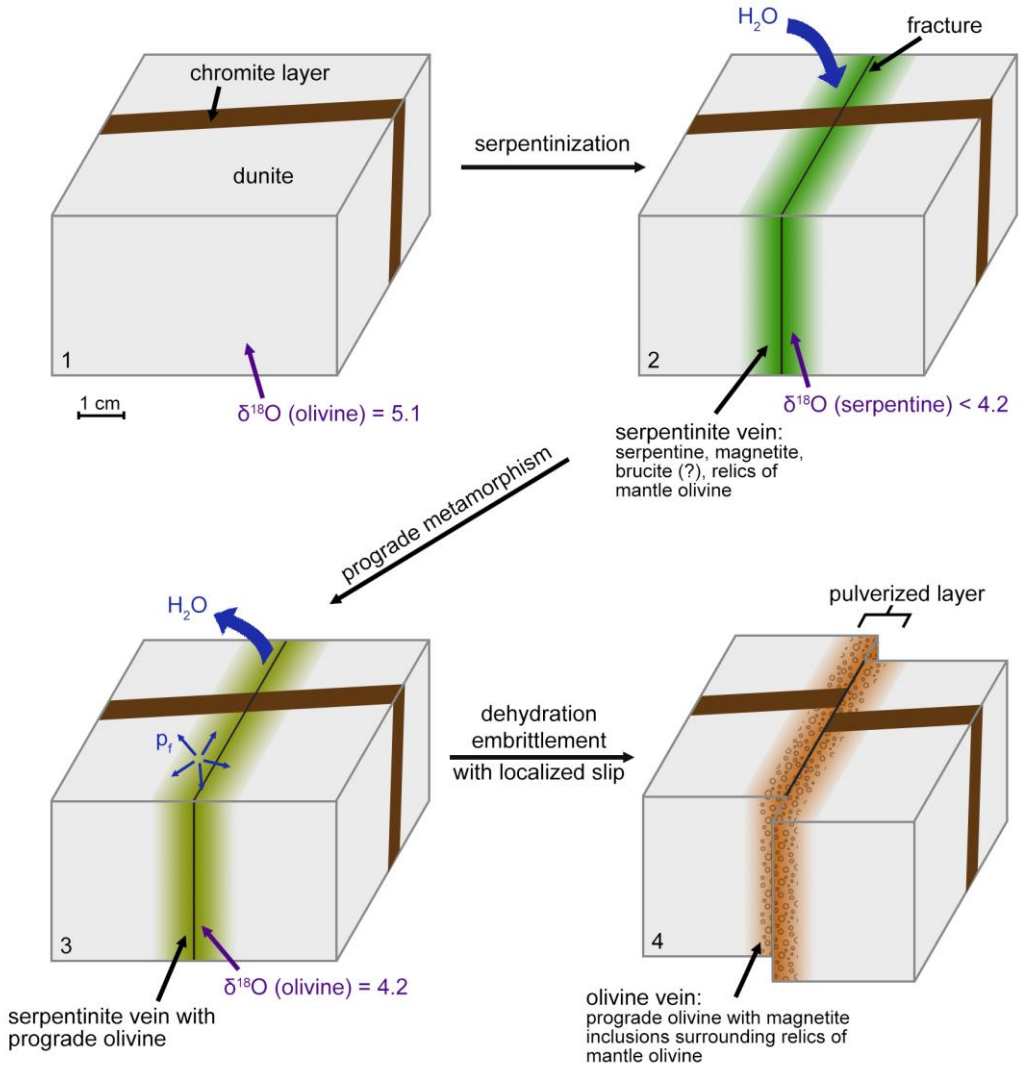

Figure 7. Schematic evolution of veining and deformation in the Leka Ophiolite Complex. Fractures in a chromite-bearing dunite provide fluid pathways along which olivine is hydrated to serpentine. During prograde metamorphism, serpentine reacts back to olivine, and the pore fluid pressure (p_f) rises. This lowers the effective normal stress and allows for localized slip on sharp fault planes in the vein centers. Propagation of a dynamic rupture leads to pulverization of prograde olivine around the slip plane. The oxygen isotope ratio decreased below 4.2‰ during serpentinization, indicating temperatures above 230 °C, and increased again during deserpentinization (see 5.1).